Karadeniz Fen Bilimleri Dergisi
The Black Sea Journal of Sciences
DOI: 10.31466/kfbd.1638041
ISSN (Online): 2564-7377
https://dergipark.org.tr/tr/pub/kfbd
Research Article / Araştırma Makalesi

Synthesis, Single Crystal X Ray Diffraction and Density Functional Theory Investigations of the p-Toluene Sulphonic Acid Complex of 3,5-Diphenyl-1H-Pyrazole

3,5-Difenil-1H-Pirazol'ün P-Toluen Sülfonik Asit Kompleksinin Sentezi, Tek Kristal X Işını Difraksiyonu Ve Yoğunluk Fonksiyonel Teorisi İncelemeleri

Adem RÜZGAR[1]*, Esvet AKBAŞ[2], Ertan ŞAHİN[3], Ebrar Nur ÖZKAN[4]

Abstract

In the present investigation, a novel complex of p-toluene sulphonic acid with 3,5-diphenyl-1H-pyrazole (p-TSA/DPP) was synthesized and subsequently characterized through various experimental techniques, including IR spectroscopy, 1H-NMR, and 13C-NMR, while the structural integrity of the compound was confirmed via single crystal X-ray diffraction analysis. Pyrazole molecules are stacked on top of each other and oriented in opposite directions, forming a layered polymeric structure by hydrogen bonding with two sulphuric acids. The density functional theory (DFT) method was used to analyze the synthetic compound's geometry at the B3LYP/6-31G (d, p) level. The single crystal XRD measurements and the optimized geometric parameters produced by the DFT calculation agree well.

Keywords: 3,5-Diphenyl-1H-pyrazole, p-Toluene sulphonic acid, XRD, DFT.

Öz

Bu çalışmada, 3,5-difenil-1H-pirazol (p-TSA/DPP) ile yeni bir p-toluen sülfonik asit kompleksi sentezlenmiş, IR spektroskopisi, 1H-NMR ve 13C-NMR ile karakterize edilmiş ve sentezlenen bileşiğin yapısal bütünlüğü tek kristal X-ışını kırınım analizi ile doğrulanmıştır. Pirazol molekülleri üst üste yığılmış ve zıt yönlere yönlendirilmiş, iki sülfürik asit ile hidrojen bağı kurarak katmanlı bir polimerik yapı oluşturmuştur. Sentetik bileşiğin geometrisini B3LYP/6-31G (d, p) seviyesinde analiz etmek için yoğunluk fonksiyonel teorisi (DFT) yöntemi kullanılmıştır. Tek kristal XRD ölçümleri ve DFT hesaplamasıyla üretilen optimize edilmiş geometrik parametreler son derece uyumlu görünmektedir.

Anahtar Kelimeler: 3,5-Difenil-1H-pirazol, p-Toluen sülfonik asit, XRD, DFT.

[1]VanYüzüncü Yıl University, Muradiye Vocational School,Van, Türkiye
[2]VanYüzüncü Yıl University, Department of Chemistry, Faculty of Science, Van,Türkiye
[3,4]Ataturk University Department of Chemistry, Erzurum, Türkiye

***Corresponding Author/Sorumlu Yazar:** aruzgar@yyu.edu.tr

Received/Geliş: 14.06.2025 **Accepted/Kabul:** 07.01.2026 **Published/Yayın:** 18.02.2026

Rüzgar, A., Akbaş, E., Şahin, E., Özkan, E. N. (2026). Synthesis, Single Crystal X Ray Diffraction and Density Functional Theory Investigations of the 3,5-Diphenyl-1H-Pyrazole's p-Toluene Sulphonic Acid Complex. *Karadeniz Fen Bilimleri Dergisi*, 16(1), 75-90. https://doi.org/10.31466/kfbd.1638041

1. Introduction

Pyrazoles are a class of heterocyclic chemicals that contain nitrogen. In recent times, the class of compounds known as substituted pyrazoles has garnered substantial interest and focus from the scientific community and industry professionals alike, primarily attributable to their multifaceted applications and significant contributions within both the medical field, where they are utilized for various therapeutic purposes, and the agricultural sector, where they play a pivotal role in enhancing crop protection and promoting sustainable agricultural practices (Akbas and Berber 2005; Sonmez et al., 2006; Zhou et al., 2024). Pyrazoles are present in the chemical structures of a number of medications, including zometapine, viagra, celebrex, cyenopyrafen, fenpyroximate, and tebufenpyrad (Roy et al., 2024; Mishra et al., 2024, Mert et al., 2025). Many pyrazoles, such as anti-pyrine, metamizole, aminopyrine, phenylbutazone, sulfinpyrazone and oxyphenbutazone have already found their clinical applications (Maddila et al., 2017; Singh et al., 2024).

The results obtained from research/application studies in which the properties of pyrazole and its derivatives have been examined in detail have revealed that these compounds can be used in both pharmacological applications and therapeutic interventions. In addition, it has been determined that pyrazole derivatives have highly critical biochemical properties such as antifungal, antimicrobial, antituberculosis, anti-inflammatory, antiviral, and anticancer. Pyrazole and its derivatives may also have an effect on the nervous system. Some derivatives are used in the treatment of anxiety, depression and other psychiatric diseases by regulating the levels of neurotransmitters in the central nervous system and promising results are obtained (Ebenezer et al., 2022; Becerra et al., 2022; Kotnala et al., 2024, Li et al., 2022).

Pyrazole derivatives can be synthesized using a variety of techniques. Some of them are given below (Karrouchi et al. 2018; Faisal et al. 2019; Ameziane El Hassani et al. 2023; Praceka et al. 2021)

Hydrazines and 1,3-diketones (Figure 1).

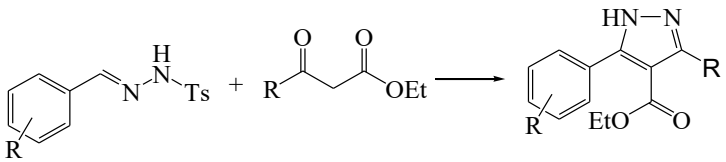

Figure 1. Synthesis from hydrazines and 1,3-diketones

From vinyl ketones (Figure 2).

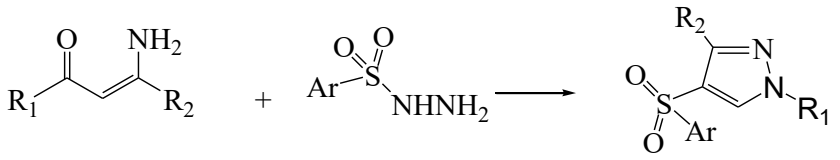

Figure 2. Synthesis from vinyl ketones

From acetylenic ketones (Figure 3).

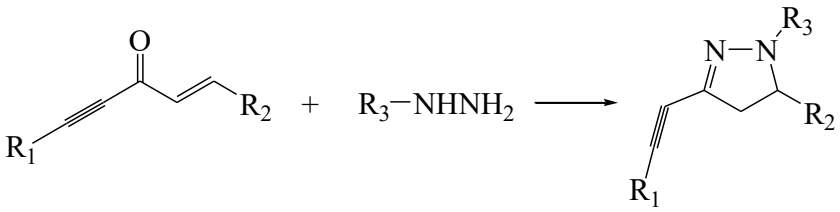

Figure 3. Synthesis from acetylenic ketones

Dipolar cycloadditions (Figure 4).

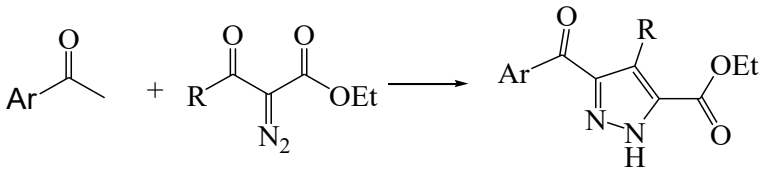

Figure 4. Synthesis from dipolar cycloadditions

From vinyldiazo ketones (Figure 5).

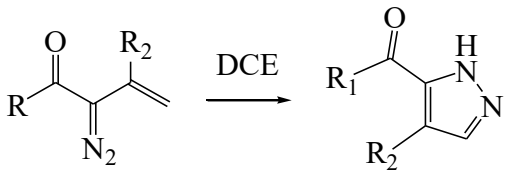

Figure 5. Synthesis from vinyldiazo ketones

From hydrazones (Figure 6).

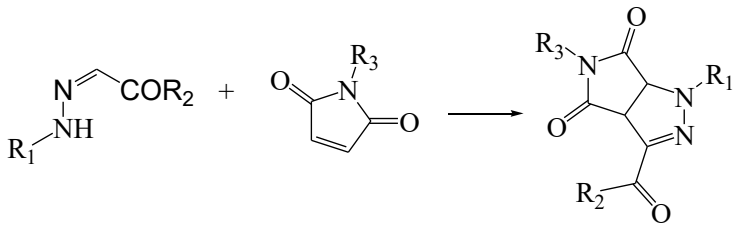

Figure 6. Synthesis from hydrazones

The utilization of quantum chemistry techniques is crucial in achieving incredibly accurate molecular geometries and forecasting diverse molecular characteristics. In the context of analyzing the intricate characteristics inherent to relatively large molecules, the implementation of density functional theory (DFT) methodologies presents an alternative utilization of computational techniques that are not only cost-effective but also efficient in their application (Akbaş, 2023). The widespread adoption of DFT within the scientific community can be attributed to its remarkable capability to comprehensively investigate various aspects of pharmaceutical compounds, including but not limited to their electronic properties, molecular structures, chemical reactivity, and the nuances of hydrogen bonding interactions.Through the meticulous execution of DFT calculations, researchers are able to delineate the molecular orbitals and geometrical configurations of organic compounds, which are fundamentally characterized by their reactivity profiles, with particular emphasis on the attributes associated with the lowest unoccupied molecular orbital energy (ELUMO), the highest occupied molecular orbital energy (EHOMO), and the significance of the frontier orbital energy difference (ΔE = ELUMO - EHOMO) in elucidating the energetic landscape of these compounds (Palafox et al. 2003).

2. Materials and Methods

In this study, the p-toluene sulphonic acid complex of 3,5-diphenyl-1H-pyrazole (Akbas et al. 2017) was synthesized using thiosemicarbazide, dibenzoylmethane and p-toluene sulphonic acid under heating in acetic acid/HCl. The product was obtained with excellent purity. The intricate architecture of the complex was meticulously elucidated through the application of various experimental methodologies, prominently featuring single crystal X-ray diffraction (XRD) techniques that provide invaluable insights into the arrangement of atoms within the crystalline structure. Furthermore, the comprehensive structural parameters for the p-TSA/DPP complex were ascertained through density functional theory (DFT) calculations employing the B3LYP hybrid functional, while utilizing the 6-31G (d, p) basis sets that facilitate a more accurate representation of electron interactions and molecular geometry. The computational analyses, which were executed with the advanced software package Gaussian09, served to complement the experimental findings by

providing theoretical predictions that align with the observed data, thereby reinforcing the validity of the structural characterization. This multi-faceted approach, combining both experimental and computational techniques, underscores the importance of integrating diverse methodologies to achieve a thorough understanding of complex molecular systems in the field of structural chemistry (Frisch et al. 2009).

3. Findings and Discussion

The p-TSA/DPP complex was obtained in a one step by the reaction of thiosemicarbazide, dibenzoylmethane and *p*-toluene sulphonic acid in acetic acid/HCl (Figure 7). 3,5-Diphenyl-1*H*-pyrazole was produced when we investigated dibenzoylmethane and thiosemicarbazide in acetic acid catalyzed *by* HCl.

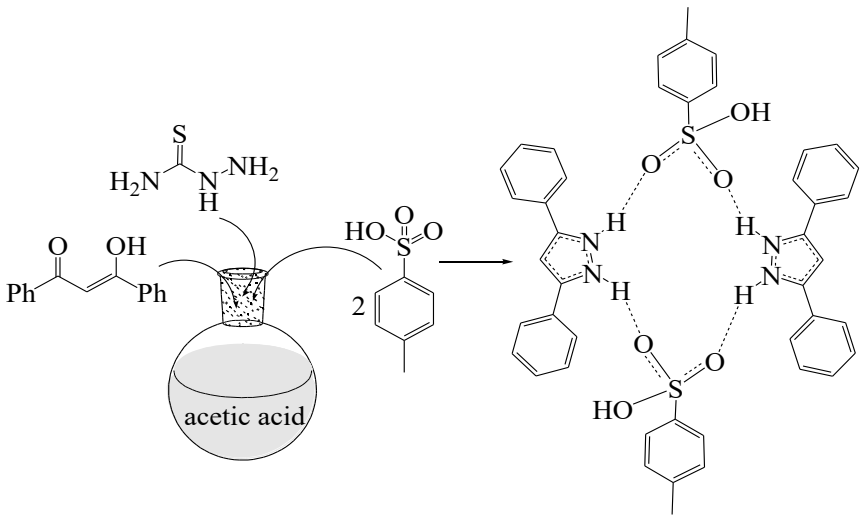

Figure 7. A one step reaction synthesis of 3, 5-diphenyl-1*H*-pyrazole/p-toluene sulphonic acid complex

The intricate and complex molecular architecture of the chemical compound in question was thoroughly elucidated and precisely characterized through the highly sophisticated and advanced technique of single crystal X-ray diffraction analysis, which is widely regarded in the field of structural chemistry for its ability to provide detailed insights into the spatial arrangement of atoms within a crystalline material (Figure 8).

The molecular architecture of the compound under investigation exhibits a crystallization pattern that conforms to the triclinic centrosymmetric space group denoted as P-1, wherein it exists in a co-crystal arrangement that comprises two distinct molecules within the asymmetric unit, thereby highlighting the complexity and symmetry inherent in its structural configuration (Figure 9).

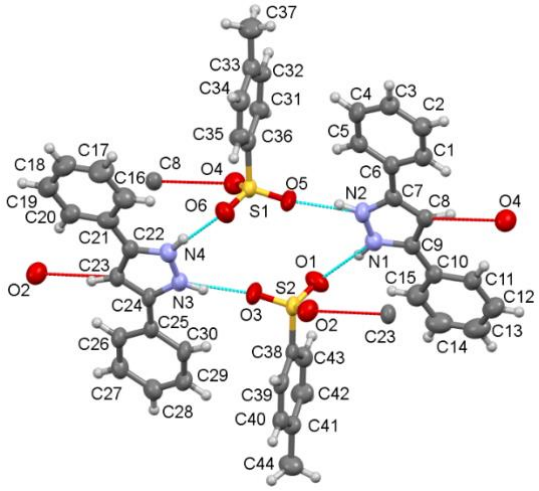

Figure 8. Molecular structure of p-TSA/DPP complex with the H-bonding geometry. The 40% likelihood level is where thermal ellipsoids are displayed. The turquoise lines show the H-bonds in the asymmetric unit and the red lines H-bonds with neighboring molecules.

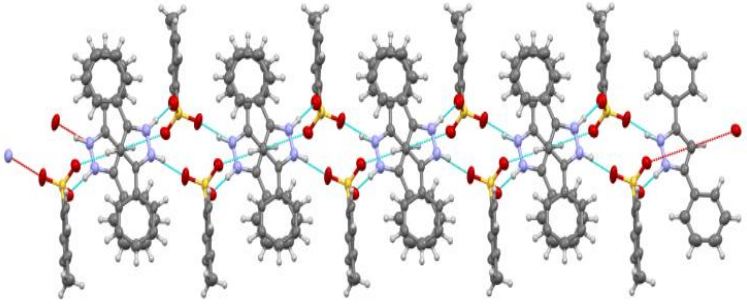

(a)

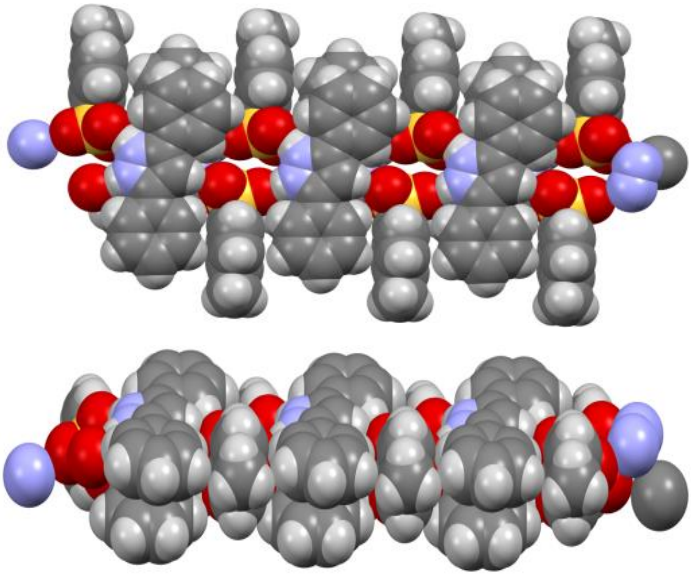

(b)

Figure 9. (a) Stacking conformer alignment in reverse and molecular hydrogen bonding (dashed lines). (b) Space-filling models with different perspective views of a stacked units consisting of hydrogen-bonded chains and Pi-Pi interactions.

The S=O (sulphonic acid) distances fall between 1.424(3) and 1.471(3) Å, which is the usual range for double bonds. The C–N bonds are between 1.365 and 1.471(3) Å, and the S=C10 double bond is 1.323(3) Å. The hydrogen atoms attached to the nitrogens in the pyrazole ring were found from the electron density (difference Fourier). N-N and C-N bond distances in the ring have double bond structure. As a result, the lone pair of electrons in the nitrogen atom is delocalized and adds to the aromatic pi-electron system, creating a resonance in the ring. In the solid state, the stabilization of the compound is predominantly achieved through the presence of robust intermolecular hydrogen bonding interactions, specifically characterized by the O3-H···O4 configuration, which exhibits a donor-acceptor distance of 2.834(3) Å, alongside the O4-H···O3 interaction that reveals a slightly shorter donor-acceptor distance of 2.794(3) Å, ultimately resulting in the emergence of a one-dimensional polymeric structure that is highly organized and exhibits significant stability. Furthermore, in relation to the structural integrity of the compound, there exist analogous hydrogen bonding interactions, namely the O3-H···O4 bond with a donor-acceptor distance of 2.874(3) Å, as well as the O4-H···O2 bond, which is characterized by an even shorter donor-acceptor distance of 2.737(3) Å, thereby contributing to the overall crystallization of the compound in a one-dimensional polymeric form that can be visually represented and analyzed as depicted in Figure 10.

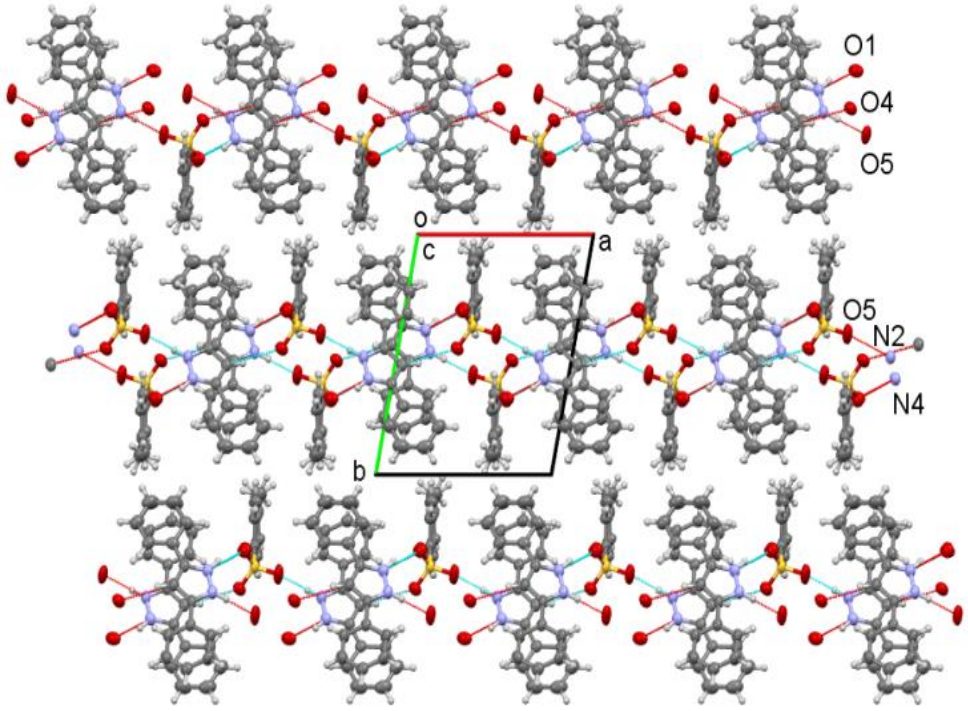

Figure 10. Packing of p-TSA/DPP within the extended crystalline network. Contacts shorter than the total of the vdW radi are indicated by dot lines.

Pyrazole molecules are stacked on top of each other and oriented in opposite directions, forming a layered polymeric structure by hydrogen bonding with two sulfuric acids. There are pi-pi interactions between phenyl rings. All hydrogen atoms in the pyrroline ring contribute to the hydrogen bond geometry. On the other hand, vdW interactions aid in the development of stable structures.

The utilization of the Hirshfeld surface (HS) alongside fingerprint plots (FPs) serves as an invaluable and insightful method that facilitates the comprehensive investigation and analysis of the intricate roles that various interatomic interactions play in determining the overall stability and integrity of molecular structures within a given system (Spackman and McKinnon 2002). In this context, the presence of a red dot on the surface of the Hirshfeld representation signifies and denotes the specific interatomic interactions and contacts that are fundamentally associated with robust and significant hydrogen bonding, which is a critical factor influencing molecular behavior. (McKinnon et al. 2004) Furthermore, the two-dimensional fingerprint map, which adeptly integrates the parameters de (the distance from a point in the Hirshfeld surface to the nearest nucleus outside the surface) and di (the distance from a point in the Hirshfeld surface to the nearest nucleus inside the surface), serves to enhance and complete the understanding of Hirshfeld surfaces by effectively summarizing and illustrating the myriad intermolecular connections that exist within the crystalline framework (Castillo et al. 2017).

To generate Fingerprint plots (FPs) in a reliable and meaningful manner, a comprehensive evaluation of the various intermolecular interactions responsible for hydrogen-bond formation was performed. For this detailed analysis, the CrystalExplorer software package, operating on crystallographic information file (CIF) data, was employed as the primary computational tool. The dnorm surfaces, which are indicative of the normalized contact distances, are elegantly represented in Figure 11, showcasing a comprehensive range that spans from a minimum value of −0.6090 Å to a maximum of 1.2034 Å, thus providing a detailed visualization of the spatial relationships among various molecular entities. The normalized contact distance, commonly referred to as dnorm, is graphically illustrated in Figure 11 employing a sophisticated color scheme that includes red, blue, and white hues; in this representation, the red regions signify areas of closer molecular contacts, which are associated with negative dnorm values, while the blue regions denote areas of more extended contacts, correlating with positive dnorm values. Moreover, it is essential to note that the weak contacts within the molecular structure are represented by patches of white color, which serve to highlight regions where the intermolecular distances are approximately equivalent to the van der Waals (vdW) separation, leading to a normalized contact distance that is roughly equal to zero, or dnorm ≈ 0 (Xu et al. 2018; Khelloul et al. 2016).

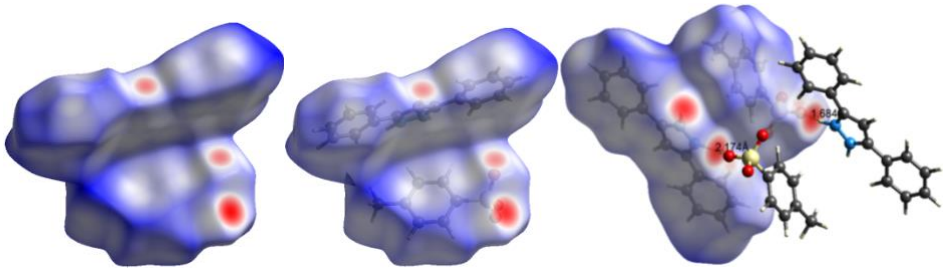

Figure 11. Dnorm overlaid onto Hirshfeld surfaces to visualize the co-crystalline intermolecular interactions.

Figure 12 illustrates the intricate arrangement wherein the hydrogen sulfide (HS) molecule envelops a transparent molecular entity situated within the crystalline medium complex, thereby providing a clear visualization of the molecular interactions present. Moreover, it is important to note that adjacent molecules that correspond to the highlighted interactions are also observable within the same field of view, thereby adding depth to our understanding of the molecular landscape. The specific contacts between oxygen and hydrogen, denoted as O-H and H-O interactions, have been accentuated to underscore the significant connections that exist between the hydrogen sulfide domains, thereby highlighting their crucial role in molecular interactions. Furthermore, the region that is depicted in color has been adorned with the dnorm feature, which serves to enhance the visual representation of the molecular architecture. It is readily apparent that the vectors, which serve to connect the oxygen atom located on the surface of the molecular structure to the two hydrogen atoms positioned externally, traverse through the very center of the red dnorm point, thus underscoring the geometric relationships at play. Additionally, it is worth noting that certain intermolecular interactions that manifest on the surface of the dnorm feature will be represented as distinct red dots, which serve as markers for specific areas of interaction. These visual indicators not only enhance our comprehension of the molecular interactions but also provide valuable insights into the nature of the forces at work within the crystalline medium. Consequently, the representation and analysis of these interactions holds significant implications for our broader understanding of molecular dynamics and structural chemistry. Ultimately, the detailed examination presented in this figure contributes to the overarching body of knowledge in the field, shedding light on the complexities inherent in molecular assembly and interaction. The O-H•••O intermolecular interactions that cause hydrogen bonding in the crystal are linked to these red dots on the surface. The HS that are mapped using the dnorm notation are represented as H•••H; H•••C/C•••H; H•••O/O•••H; C•••C and N•••. The hydrogen contacts that were most prominent on the overall HS were C/C•••N and N•••H/H•••N. Figure 13 describes the 2D fingerprint plot and the contribution of each kind of interaction. The highest contribution (43.2%) to the HS is made by H•••H contacts, which are broadly distributed and highly concentrated in the center sector, as shown in Figure 13 with $d_e + d_i \sim 2.5$ Å. The latter contributions come from 23.2% O-H•••O hydrogen bonding and are represented by a pair of symmetrical sharp

spikes in the 2.55 Å region (Figure 13). The N•••H interaction (0.2%) also appears in the FPs as two distinct broad spikes at d_i = 1.2 Å and d_i = 1.8 Å (Figure 13). Additionally, Figure 13 shows the C•••H/H•••C interaction formed by the total HS (20.9%) presented by the two pairs of wings in the fingerprint plot.

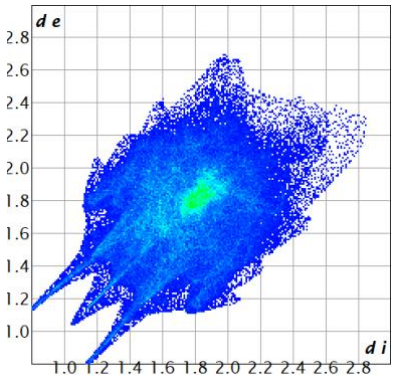

Figure 12. The HS in the co-crystalline was influenced by FPsof the numerous intercontacts and the percentage of different intermolecular interactions.

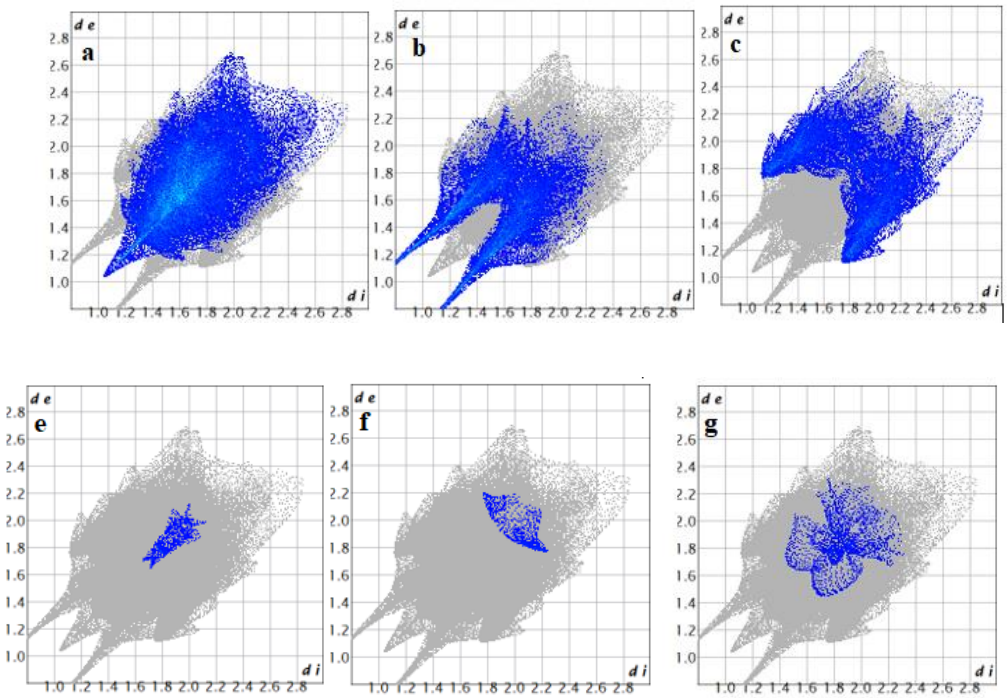

Figure 13. 2D Finger print drawing of molecule co-crystalline (a) H•••H (%43.2), (b) H •••O/O•••H (%23.2), (c) H•••C/C•••H (%20.9), (d) C•••C (%8.8) (e) N···C/C···N (%0.9), (f) O···O (%0.8) and (g) H•••N/N•••H (%0.2).

The analysis employing hydrogen bond strength (HS) was utilized to validate the contributions of diverse intermolecular interactions. Through this methodology, the hydrogen bonding and additional weak intermolecular interactions present in the crystal structure were scrutinized. The HS

diagrams presented below substantiate the existence of the non-covalent interactions depicted in Figure 14.

In conjunction with the analysis conducted through Hirshfeld surface (HS) methodology, supplementary analytical techniques such as the shape index and the examination of curved surfaces were systematically employed in order to meticulously observe and quantitatively assess the various similarities and differences that exist in intermolecular interactions throughout the comprehensive crystal structure under investigation. The weak intermolecular interactions, which are primarily characterized by hydrogen bonding interactions such as H···O, H···N, H···C, and H···H, exhibit distinctive traits wherein the mutual contacts for H···O interactions manifest as sharply defined needle-like structures, with the distance parameters de + di approximately equaling 2.8 Å, as illustrated in Figures while for H···N interactions of the Hirshfeld surface, these interactions appear as two dispersed wings with a distance measurement of de + di approximately 3.1 Å, indicating a separation that exceeds the van der Waals radii of the hydrogen atoms involved, as depicted in Figure 13, where it is noted that di + de is greater than 2.75 Å. This particular observation suggests that such weak interactions do not contribute significantly to the overall crystal packing of the molecules under consideration in this study. The intricate details of these intermolecular forces are critical for understanding the stability and arrangement of the molecular framework within the crystalline environment. Therefore, the implications of these findings extend beyond mere structural characterization, offering insights into the broader physical and chemical properties inherent to the crystal system being analyzed. The most of the generated surface's contribution comes from interatomic contacts of H···H, which display a symmetrical sharp needle with $d_e + d_i \simeq 2.4$ Å. This suggests that short contacts of H···H have a considerable impact on molecular packing and crystal structure stabilization.

Shape index surfaces are mapped between -1 and 1 Å. Red and blue triangles indicate π–π interactions. Parts of the co-crystal (a) show the interactions of the –π components on the red triangle indicated by the arrows. The curvature surfaces are represented within the range of -4 to 0.4 Å. Planar areas underscore the involvement of rings in stacking interactions. (Spackman et al. 2021)

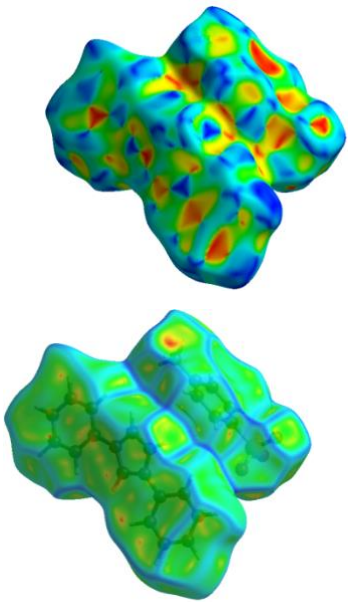

Figure 14. Shape index and Curvedness HS maps view of co-crystalline.

Selected structural and physicochemical properties of p-TSA/DPP were subjected to theoretical analysis. Geometry optimizations were carried out within the framework of density functional theory (DFT) using the B3LYP functional in conjunction with the 6-31G(d,p) basis set. The calculated total energies, frontier molecular orbital energies, and the corresponding HOMO–LUMO energy gaps are summarized in Tab. 1.

Table 1. Theoretical information via QCC (eV)

Tot. Ener. (eV)	$E_H(eV)$	$E_L(eV)$	$\Delta E_{gap}(eV)$	Dipole Moment
86.209	19.9314	-3.5321	16.3993	4.659469 D

Figure 15 provides a representative optimized geometric structure together with the frontier orbitals. Whereas the electron density of LUMO appears to be mostly localized in the sulphonic acid segment, that of HOMO appears to be confined in the pyrazole ring part.

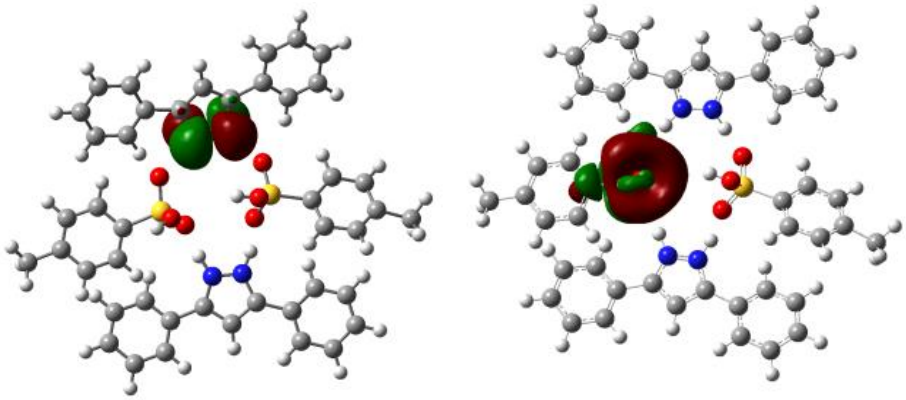

Figure 15. The optimized structures, frontier HOMO and LUMO orbital.

Figure 16 presents the three-dimensional electrostatic potential (ESP) mapped onto the molecular orbitals, namely the Highest Occupied Molecular Orbital (HOMO) and the Lowest Unoccupied Molecular Orbital (LUMO), together with the corresponding contour and total electron density obtained from Self-Consistent Field/Electrostatic Potential (SCF/ESP) calculations using a planar grid representation. In the molecular electrostatic potential map, regions with the most negative electrostatic potential are highlighted in red, indicating electron-rich areas, whereas less negative or relatively positive regions are shown in lighter colors.

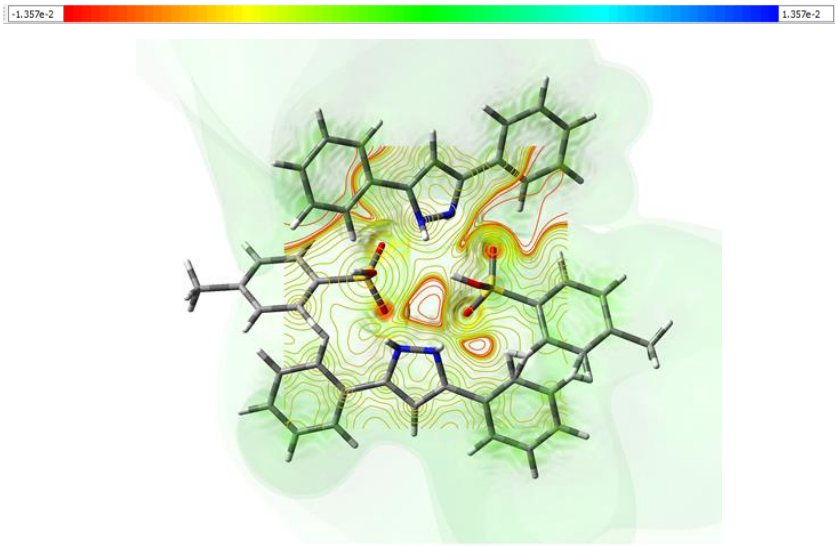

Figure 16. The optimized structures, frontier HOMO and LUMO orbital.

4. Conclusions and Recommendations

In conclusion, we have successfully synthesized the complex of p-toluene sulphonic acid combined with 3,5-diphenyl-1H-pyrazole, which we refer to as p-TSA/DPP, by employing a novel

method that showcases significant advancements in our approach. The structural integrity and configuration of this complex were meticulously confirmed through X-ray diffraction (XRD) analysis, providing us with reliable data regarding its three-dimensional arrangement. Within this particular complex, it is noteworthy to mention that there exists not one, but two distinct molecules situated within the asymmetric unit, which plays a crucial role in the overall properties of the compound. Additionally, we observed that one-dimensional polymeric chains were effectively formed, which are held together by robust intermolecular O-H···O hydrogen bonding interactions, extending significantly along the a-axis and contributing to the structural stability. To further elucidate the geometry of the synthesized compound, we conducted an extensive examination utilizing the B3LYP/6-31G (d, p) level of theory, which is a prominent method within the realm of density functional theory (DFT). This meticulous analysis not only enhances our understanding of the compound's electronic structure but also provides valuable insights into its potential applications in various fields of research. Thus, the integration of experimental and theoretical approaches has yielded a comprehensive understanding of the p-TSA/DPP complex, paving the way for future studies in this area of chemistry. Whereas the electron density of LUMO is mostly found in the sulphonic acid segment, the electron density of HOMO is centered on the pyrazole ring moiety. The single-crystal X-ray diffraction (XRD) results show good agreement with the optimized geometric parameters. Intramolecular charge transport can be effectively described in terms of the HOMO–LUMO energy levels. Furthermore, the molecular electrostatic potential (MEP) analysis was carried out to predict the reactive sites within the molecule.

Syntheses of the 3,5-diphenyl-1H-pyrazole-p-toluene sulphonic acid complex (p-TSA/DPP)

For around 12 hours, an equimolar combination of p-toluene sulphonic acid (2 mmol), thiosemicarbazide (1 mmol), and dibenzoylmethane (1 mmol) was refluxed in 10 ml of ethanol. Following its formation, the product was recrystallized from ethanol to yield 48% efficiency. En: 225-226ºC, IR (cm^{-1}) : 3143, 3061, 2899, 2758, 1625, 1597, 1467, 1421, 1165. ^{1}H-NMR (DMSO-*d6*): δ (ppm) 7.85 (dd, 1H, NH), 7.80 (d, 1H, NH), 7.30-7.50 (m, 30H, Harm), 7.20 (dd, 1H, =CH), 2.30 (s, 3H, CH_3). ^{13}C-NMR (DMSO-d6): δ (ppm) 31.00, 99.60, 125.07, 125.75, 126.40, 127.20, 127.54, 127.77, 128.32, 128.81, 129.40, 129.55, 130.30, 130.52, 130.64, 149.20.

Single-crystal X-ray diffraction analysis was performed for the p-TSA/DPP complex in order to elucidate its solid-state structure. Data were collected on a four-circle Rigaku R-AXIS RAPID-S diffractometer equipped with a two-dimensional imaging plate detector using graphite-monochromated Mo-Kα radiation (λ = 0.71073 Å). The measurements were carried out employing an oscillation scan mode with a step width of Δw = 5°. Unit cell parameters were refined by the least-squares method using all reflections with $F^2 > 2\sigma(F^2)$. Data reduction, intensity integration, Lorentz and polarization corrections, as well as cell refinement were carried out using the CrystalClear

software package. The structure was solved by direct methods using SHELXS-2013 and subsequently refined by full-matrix least-squares refinement on F^2 with SHELXL-2013. All non-hydrogen atoms were refined anisotropically, while hydrogen atoms were placed at calculated positions and refined using a riding model with isotropic displacement parameters. No significant residual electron density peaks were observed in the final difference Fourier maps. The p-TSA/DPP complex crystallizes in the triclinic crystal system with space group P-1 (Z = 2), and representative geometric and crystallographic parameters confirm the reliability of the refined structure. Complete crystallographic data for this structure have been deposited with the Cambridge Crystallographic Data Centre under deposition number CCDC-2223989, where they can be accessed free of charge.

Authors' Contributions

All authors contributed equally to the study.

Statement of Conflicts of Interest

There is no conflict of interest between the authors.

Statement of Research and Publication Ethics

The author declares that this study complies with Research and Publication Ethics.

References

Akbaş, E. (2023). DFT investigation of adsorption of pyrimidine derivatives on graphene oxide. *Journal of ata-chem*, 3(2).

Akbas, E., & Berber, I. (2005). Antibacterial and antifungal activities of new pyrazolo [3, 4-d] pyridazin derivatives. *European Journal of Medicinal Chemistry*, 40(4), 401-405.

Akbas, E., Celikezen, F. C., Turkez, H., Ozdemir, O., Ruzgar, A., Ergan, E., & Sahin, E. (2017). Synthesis of the 3, 5-diphenyl-1 H-pyrazole and cytogenetic and oxidative alterations after exposure of cultured human whole blood cells. *Cogent Chemistry*, 3(1), 1344115.

Ameziane El Hassani, I., Rouzi, K., Assila, H., Karrouchi, K., & Ansar, M. H. (2023). Recent advances in the synthesis of pyrazole derivatives: a review. *Reactions*, 4(3), 478-504.

Becerra, D., Abonia, R., & Castillo, J. C. (2022). Recent applications of the multicomponent synthesis for bioactive pyrazole derivatives. *Molecules*, 27(15), 4723.

Castillo, M. V., Rudyk, R. A., Davies, L., & Brandán, S. A. (2017). Analysis of the structure and the FT-IR and Raman spectra of 2-(4-nitrophenyl)-4H-3, 1-benzoxazin-4-one. Comparisons with the chlorinated and methylated derivatives. *Journal of Molecular Structure*, 1140, 2-11.

Ebenezer, O., Shapi, M., & Tuszynski, J. A. (2022). A review of the recent development in the synthesis and biological evaluations of pyrazole derivatives. *Biomedicines*, 10(5), 1124.

Faisal, M., Saeed, A., Hussain, S., Dar, P., & Larik, F. A. (2019). Recent developments in synthetic chemistry and biological activities of pyrazole derivatives. *Journal of Chemical Sciences*, 131, 1-30.

Karrouchi, K., Radi, S., Ramli, Y., Taoufik, J., Mabkhot, Y. N., Al-Aizari, F. A., & Ansar, M. H. (2018). Synthesis and pharmacological activities of pyrazole derivatives: A review. *Molecules*, 23(1), 134.

Khelloul, N., Toubal, K., Benhalima, N., Rahmani, R., Chouaih, A., Djafri, A., & Hamzaoui, F. (2016). Crystal structure, Hirshfeld surface analysis and computational studies of thiazolidin-4-one derivative:(Z)-5-(4-Chlorobenzylidene)-3-(2-ethoxyphenyl)-2-thioxothiazolidin-4-one. *Acta Chim. Slov*, 63, 619-626.

Kotnala, M., Singh, G., Singh, K., Nath, R., Panda, K. C., Kumar, A., & Dutta, S. (2024). Exploring the Synthetic Strategies and Biological Activities of Pyrazole Derivatives. *Naturalista Campano*, 28(1), 3238-3248.

Li, G., Cheng, Y., Han, C., Song, C., Huang, N., & Du, Y. (2022). Pyrazole-containing pharmaceuticals: target, pharmacological activity, and their SAR studies. *RSC Medicinal Chemistry*, 13(11), 1300-1321.

Maddila, S., Jonnalagadda, S. B., Gangu, K. K., & Maddila, S. N. (2017). Recent advances in the synthesis of pyrazole derivatives using multicomponent reactions. *Current Organic Synthesis*, 14(5), 634-653.

McKinnon, J. J., Spackman, M. A., & Mitchell, A. S. (2004). Novel tools for visualizing and exploring intermolecular interactions in molecular crystals. *Acta Crystallographica Section B: Structural Science*, 60(6), 627-668.

Mert, S., Demir, Y., Sert, Y., Kasımoğulları, R., & Gülçin, İ. (2025). Synthesis, biological evaluation and molecular docking of novel pyrazole derivatives as multitarget acetylcholinesterase and carbonic anhydrase inhibitors. *Journal of Molecular Structure*, 1319, 139472.

Mishra, A., Talukdar, M., Krishna, G. R., & Begari, E. (2024). One-Pot Synthesis of Pyrazoles from Sulfonyl Hydrazides and Alkynyl Ketones Using Environmentally Benign Sulfonium Iodate (I) Reagent. *ChemistrySelect,* 9(38), e202403249.

M.J. Frisch, G.W. Trucks, H.B. Schlegel, G.E. Scuseria, M.A. Robb, J.R. Cheeseman, G. Scalmani, V. Barone, B. Mennucci, G.A. Petersson, H. Nakatsuji, M. Caricato, X. Li, H.P. Hratchian, A.F. Izmaylov, J. Bloino, G. Zheng, J.L. Sonnenberg, M. Hada, M. Ehara, K. Toyota, R. Fukuda, J. Hasegawa, M. Ishida, T. Nakajima, Y. Honda, O. Kitao, H. Nakai, T. Vreven, J.A. Montgomery, Jr.J.E. Peralta, F. Ogliaro, M. Bearpark, J.J. Heyd, E. Brothers, K.N. Kudin, V.N. Staroverov, R. Kobayashi, J. Normand, K. Raghavachari, A. Rendell, J.C. Burant, S.S. Iyengar, J. Tomasi, M. Cossi, N. Rega, J.M. Millam, M. Klene, J.E. Knox, J.B. Cross, V. Bakken, C. Adamo, J. Jaramillo, R. Gomperts, R.E. Stratmann, O. Yazyev, A.J. Austin, R. Cammi, C. Pomelli, J.W. Ochterski, R.L. Martin, K. Morokuma, V.G. Zakrzewski, G.A. Voth, P. Salvador, J.J. Dannenberg, S. Dapprich, A.D. Daniels, O. Farkas, J.B. Foresman, J.V. Ortiz, J. Cioslowski, and D.J. Fox. Gaussian, Inc., Wallingford CT, USA, 2009.

Palafox, M. A., Rastogi, V. K., Tanwar, R. P., & Mittal, L. (2003). Vibrational frequencies and structure of 2-thiouracil by Hartree–Fock, post-Hartree–Fock and density functional methods. *Spectrochimica Acta Part A: Molecular and Biomolecular Spectroscopy*, 59(11), 2473-2486.

Praceka, M. S., Megantara, S., Maharani, R., & Muchtaridi, M. (2021). Comparison of various synthesis methods and synthesis parameters of pyrazoline derivates. *Journal of Advanced Pharmaceutical Technology & Research*, 12(4), 321-326.

Roy, S., Chatterjee, R., Kisan, P., & Dandela, R. (2024). Ultrasound-assisted synthesis of 1, 5-disubstituted pyrazoles via HFIP-mediated cascade cyclization of enaminones with aryl hydrazine. *Tetrahedron Letters*, 149, 155277.

Spackman, M. A., & McKinnon, J. J. (2002). Fingerprinting intermolecular interactions in molecular crystals. *CrystEngComm*, 4(66), 378-392.

Spackman, P. R., Turner, M. J., McKinnon, J. J., Wolff, S. K., Grimwood, D. J., Jayatilaka, D., & Spackman, M. A. (2021). CrystalExplorer: a program for Hirshfeld surface analysis, visualization and quantitative analysis of molecular crystals. *Journal of Applied Crystallography*, 54(3), 1006-1011.

Singh, S., Singh, K., & Tahlan, S. (2024). A comprehensive review on synthetic strategy and MOA of marketed drugs having therapeutically potential chemical entity pyrazole. *Journal of the Iranian Chemical Society*, 21(10), 2531-2564.

Sönmez, M., Berber, İ., & Akbaş, E. (2006). Synthesis, antibacterial and antifungal activity of some new pyridazinone metal complexes. *European Journal of Medicinal Chemistry*, 41(1), 101-105.

Xu, X., Liu, C., Sun, Z., Cao, T., Zhang, Z., Wang, E., ... & Liu, K. (2018). Interfacial engineering in graphene bandgap. *Chemical Society Reviews*, 47(9), 3059-3099.

Zhou, J., Zhou, Q. Q., & Wan, J. P. (2024). Recent advances in multicomponent synthesis of pyrazoles. Organic & Biomolecular Chemistry.